A 3-Dimensional Picture of Energy Transport in Fast Flows Through Earth's Magnetotail

K. C. Barik*(1), and C. C. Chaston(1)
(1) Space Sciences Laboratory, University of California, Berkeley, CA, USA

Abstract

A comprehensive statistical analysis of energy transport through Earth's magnetotail is conducted using six years of observations from the Magnetospheric Multiscale (MMS) mission. This analysis involves a thorough decomposition of energy contributions, including the previously overlooked heat flux and enthalpy flux derived from the full pressure tensor, yielding a detailed three-dimensional (3-D) representation of magnetotail energy transport. Results reveal a competitive interplay between the Poynting flux and enthalpy flux in driving total energy transport, while the previously neglected heat flux emerges as a significant contributor to the total energy flux, surpassing the bulk kinetic energy flux. Moreover, the study uncovers persistent spatial asymmetries in energy transport distribution, offering valuable insights into magnetospheric dynamics.

1 Introduction

Energy transport through Earth's magnetotail is primarily carried by fast flows, characterized as ion flows with speeds exceeding the typical convection speed of 50 km/s [1, 2]. These high-speed flows carry energy both Earthward and tail-ward from the reconnection point, where magnetic energy undergoes conversion into thermal energy through the reconfiguration of magnetic field lines. The transported energy manifests as enthalpy flux from the x-point in the distant tail to the near-Earth region, where ion flows decelerate due to the formation of dipolarization fronts (DFs) and the conversion of thermal to magnetic energy. Additionally, energy is directed to auroral altitudes in the form of Poynting flux or field-aligned currents (FACs), significantly influencing auroral dynamics. As a result, energy input from the reconnection point is distributed across the magnetosphere in various forms. Understanding the intricacies of energy transport in Earth's magnetotail is crucial for unraveling the complexities of magnetospheric dynamics.

Earlier studies focused primarily on Poynting flux and kinetic energy flux as the primary components of energy transport [3]. Subsequent research by [1] expanded the analysis to include enthalpy flux. More recently, [2] investigated the total energy flux derived from the moment of ion distribution. However, all of these studies overlooked the heat flux. While emphasizing the significance of fast flows for energy transport, there remains a need for deeper physical insights achieved by decomposing the energy flux into its elemental electromagnetic and kinetic components. In this letter, we address this gap by conducting a statistical analysis of MMS measurements, offering a comprehensive 3-D depiction of energy transport across Earth's magnetotail.

2 Event Selection

We have used six years of night phase data of the MMS mission from 2017-2022 to investigate the energy transport in Earth's magnetotail. Night phases of MMS are selected by visual inspection of the MMS orbit plot. A database is created to examine the energy transport in Earth's magnetotail at micro-scale. Events are selected by measurements separated by times defined by advection in the flow corresponding to a distance of $2\pi\rho_i$, where $\rho_i = \left(\frac{mv_{th}}{qB}\right)$ denotes the ion gyro radius and m, q and v_{th} are respectively the mass, charge, and thermal speed of the protons. Furthermore, fast flow events are identified based on ion flow speed exceeding the convection speed threshold of 50 km/s. [1, 2]. Finally, the data points corresponding to the outer low latitude boundary layer (LLBL) and inner LLBL are excluded by limiting the ion number density to $n_i = 10\ cm^{-3}$ and $n_i \geq 1\ cm^{-3}$, respectively [7]. With these selection criteria, a total of 457515 data points are procured in our database.

3 Analysis

In this study, the total energy flux is decomposed into (i) the electromagnetic energy, i.e., Poynting flux, (ii) thermal energy fluxes including the enthalpy flux and heat flux, and (iii) the bulk kinetic energy flux. The temporal evolution of total energy density (W) is defined by

$$\frac{dW}{dt} = -\nabla.\left[\frac{\rho v^2}{2}\mathbf{v} + \left(\frac{\mathbf{v}Tr\left(\overleftrightarrow{P}\right)}{2} + \frac{\gamma P}{\gamma - 1}\mathbf{v}\right) + Q_H + \frac{1}{\mu_0}\left(\mathbf{E}\times\mathbf{B}\right)\right] \quad (1)$$

On RHS, the first term represents the bulk kinetic energy flux, where $\rho = n_i m_i$ indicates the ion mass density and $\mathbf{v}$ is the ion flow speed. The second term within the parenthesis gives expression for the enthalpy flux, the first part of which is computed from the product of ion flow velocity with the pressure tensor $(\overleftrightarrow{P})$ directly provided by the Fast Plasma Investigation (FPI) onboard MMS. In the second part, $P = n_i k_B T_i$ represents the ion thermal pressure, where k_B denotes the Boltzmann's constant, T_i is ion temperature and γ indicates the polytropic index. Third term (Q_H) represents heat flux directly measured from FPI instrument. Poynting flux denoted by the last term on RHS is calculated using the electric [fast-survey mode Electric Double Probe (EDP) data] [5] and magnetic field [survey mode Flux Gate Magnetometer (FGM) data] [4]. The use of FGM data suffices the study of energy transport at micro-scale since the **B** field fluctuations at $2\pi\rho_i$ or smaller scale is dominated by FGM. **E** and **B** fields are filtered and down-sampled to synchronize with FPI [6] for the statistical survey. It is noteworthy that current study is limited to energy transport in the range of 10 eV to 30 keV as FPI measures particles data in that range.

4 Results

The absolute value of various energy fluxes are measured at different geocentric solar magnetospheric (GSM) locations of the Earth's magnetotail. Each plane (XY, XZ, and YZ) is segmented into bins of size 1 $R_E \times 1$ R_E, where R_E represents the radius of Earth. Mean energy flux values within each bin are plotted to illustrate the spatial distribution. In the figures, the color bar indicates the in-situ energy flux values measured in mW/m^2 corresponding to the (abscissa, ordinate) pair in the figures. The color bar range is consistent across all figures for ease of comparison.

Figure 1(a) demonstrates the distribution of Poynting flux in the geomagnetic equatorial XY-plane in GSM coordinates. The region with $X_{GSM} < -15$ R_E is classified as the distant magnetotail, while -15 $R_E \geq X_{GSM} \leq -5$ R_E represents the near-Earth magnetotail region. Additionally, regions with $|Y_{GSM}| \leq \pm 12$ R_E are designated as central, while those with $|Y_{GSM}| \geq \pm 12$ R_E constitute the edge of the distribution plane. In the central XY-plane, Poynting flux gradually increases from the distant magnetotail to the near-Earth region, peaking at the latter. Conversely, the Poynting flux decreases from the central region towards the edge of the XY-plane. The concentration of enthalpy flux in the near-Earth magnetotail region of the central plane is relatively high compared to the distant magnetotail region (Figure 1(b)), which is predominantly more localized in the duskward sector ($+Y_{GSM}$ direction) than the dawnward sector ($-Y_{GSM}$ direction). A detailed comparison between the Poynting and enthalpy fluxes reveals their respective dominance regions, as discussed in Section 5. Unlike the Poynting flux, which peaks close to the origin in the Y_{GSM}-axis, the enthalpy flux attains its maximum away from the origin. The bulk kinetic energy flux exhibits relatively larger values in the duskward sector of the near-Earth magnetotail region and the dawnward sector of the distant magnetotail region compared to their counterparts (Figure 1(c)). In contrast, the heat flux in the central region of the XY-plane appears more uniform compared to other energy fluxes (Figure 1(d)). The value of the heat flux at the edge of the XY-plane is relatively small compared to the central region.

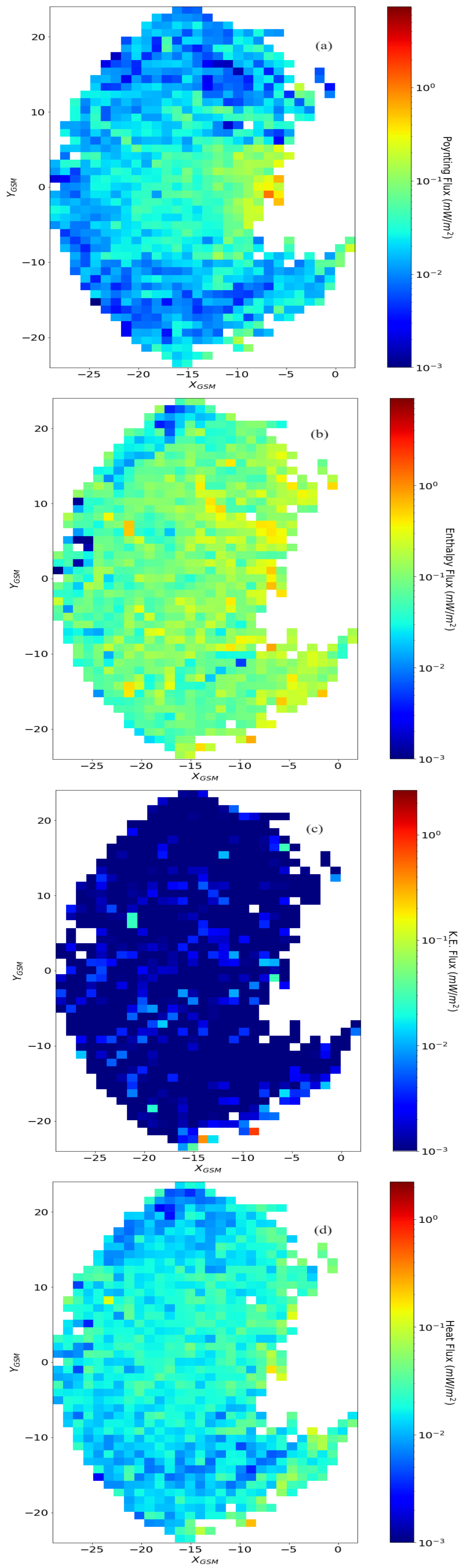

Figure 1. Shows the variations of (a) Poynting flux, (b) enthalpy flux, (c) bulk kinetic energy flux, and (d) heat flux in XY-plane

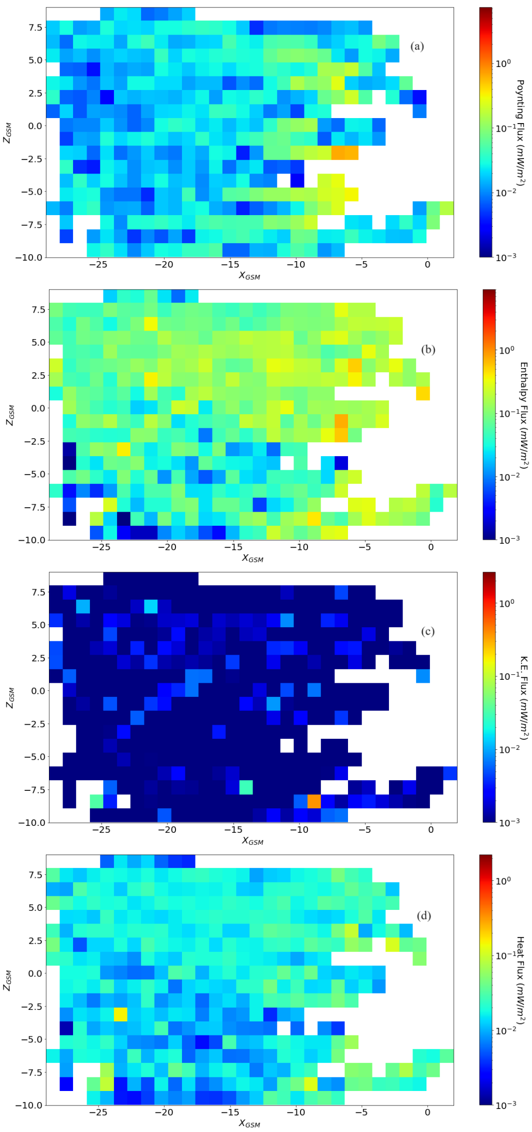

Figure 2. Shows the variations of (a) Poynting flux, (b) enthalpy flux, (c) bulk kinetic energy flux, and (d) heat flux in XZ-plane

Fig. 2 illustrates the distribution of different energy fluxes in the meridional (YZ) plane. In the near-Earth magnetotail region, the distribution of Poynting flux exhibits north-south asymmetry, with the flux predominantly concentrated in the southward direction (along the $-Z_{GSM}$) compared to the northward direction (along the $+Z_{GSM}$) (Figure 2(a)). Conversely, the value of the enthalpy flux in the northward direction over the entire magnetotail region (both distant and near-Earth) is relatively large compared to the southward direction (Figure 2(b)). Both the heat flux (Figure 2(d)) and bulk kinetic energy flux (Figure 2(c)) exhibit similar north-south asymmetry characteristics to the enthalpy flux, although with relatively smaller flux magnitudes.

The distribution of various energy fluxes in the YZ-plane is depicted in Figure 3. Poynting flux is predominantly concentrated in a specific range of Y_{GSM}, spanning from

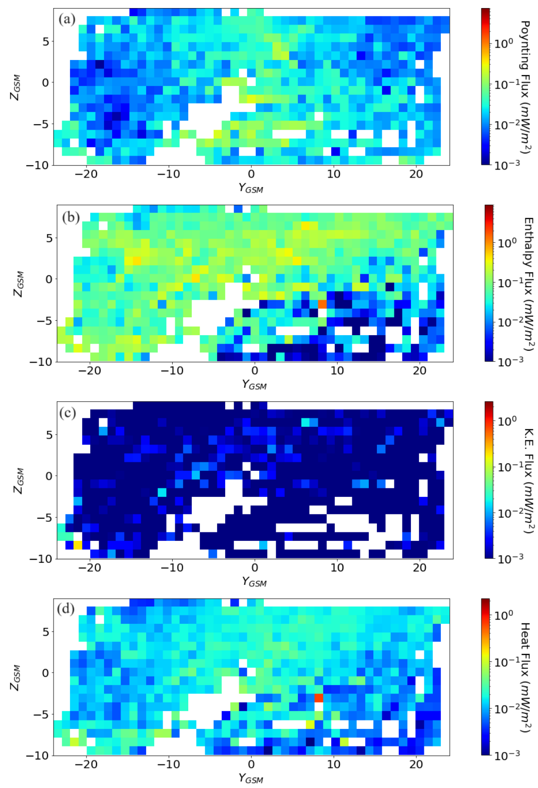

Figure 3. Shows the variations of (a) Poynting flux, (b) enthalpy flux, (c) bulk kinetic energy flux, and (d) heat flux in YZ-plane

$+12\ R_E$ to $-12\ R_E$ and covering the entire Z_{GSM} range (Figure 3(a)). Enthalpy flux is more localized in the northern region compared to the southern region (Figure 3(b)). Furthermore, bulk kinetic energy flux, although of small magnitude, appears to be concentrated in the Y_{GSM} range, spanning from $+7\ R_E$ to $-10\ R_E$ (Figure 3(c)). Heat flux exhibits a similar trend to the enthalpy flux, albeit with a relatively smaller magnitude (Figure 3(d)).

5 Discussions

Our database contains a total of 457,515 data points. We classify the magnetotail into two regions based on ion plasma beta (β_i) values, as defined by [1]. The region where $\beta_i \geq 0.5$ is termed the inner plasma sheet (IPS), which comprises most of the inner central plasma sheet (ICPS) and some of the outer central plasma sheet (OCPS). Conversely, the region where $\beta_i < 0.5$ is labeled the outer plasma sheet (OPS), encompassing most of the plasma sheet boundary layer (PSBL) and some OCPS. In our dataset, we find 321,156 data points in the IPS and 136,359 data points in the OPS. Table 1 details the variations of different energy fluxes in the IPS and OPS regions under various flux dominance conditions. The shorthand notations used for various energy fluxes in the table are: Poynting flux (SF), enthalpy flux (EF), bulk kinetic energy flux (KE), and heat flux (HF).

In the IPS ($\beta_i \geq 0.5$) region, the enthalpy flux surpasses

Table 1. Statistics of different energy flux variations in the IPS ($\beta_i \geq 0.5$) and in the OPS ($\beta_i < 0.5$) region. Total number of data points in the IPS and OPS are 321156, and 136359, respectively.

Cond. of Flux Variations	For $\beta_i \geq 0.5$ No of data points	% of Occurrence	For $\beta_i < 0.5$ No of data points	% of Occurrence
$SF > EF$	27558	8.58	105282	77.21
$SF > HF$	124811	38.86	121365	89.00
$SF > KE$	310802	96.77	136100	99.81
$HF > EF$	21376	6.66	59804	43.86
$HF > KE$	318357	99.12	135641	99.47
$KE > EF$	0	0	31	0.02

the other three energy fluxes. Specifically, it is larger than the Poynting flux, heat flux and bulk kinetic energy flux in 91.42 %, 93.34 %, and (100 %) of the events, respectively. Additionally, the heat flux is larger than the bulk kinetic energy flux (almost 99.12 % of the events), and Poynting flux (in 61.14 % of the events). Hence, in the IPS region, the hierarchy in flux distribution is as follows: $EF > HF > SF > KE$.

In the OPS ($\beta_i < 0.5$), the Poynting flux notably contributes significantly to the total energy flux compared to the other three energy fluxes. It exhibits relatively larger values than the enthalpy flux, heat flux, and bulk kinetic energy flux in 77.21 %, 89.00 %, and 99.81 % of the events, respectively. Furthermore, in 56.14 % of the events, enthalpy flux surpasses the heat flux. Consequently, the hierarchy in flux distribution in OPS is of the order $SF > EF > HF > KE$.

6 Conclusions

We have utilized six years (2017-2022) of MMS night phase data to examine the energy transport in Earth's magnetotail. Total pressure tensor is included in the calculation of enthalpy flux, and heat flux is considered for the first time. These results add novelty to the existing literature and offer deeper insights into Earth's magnetotail dynamics. Surprisingly, the heat flux, which was neglected in earlier studies assuming it to be negligible, is found to contribute significantly to the total energy flux of the magnetotail. Furthermore, this study presents the distribution of various energy fluxes in three-dimensional (3-D) space.

In the XY-plane, the enthalpy flux and bulk kinetic energy flux exhibits dawn-dusk asymmetry in the near-Earth magnetotail region. It could be due to the duskward motion of ions at the near-earth region. The heat flux distribution over the XY-plane appears to be very uniform. In the XZ-plane, Poynting flux displays north-south asymmetry in the near-Earth region, while the other three energy fluxes exhibit north-south asymmetry across the entire magnetotail. In YZ-plane, each energy flux exhibits north-south asymmetry, albeit their region of localization is different [Sec 4]. This could be due to tilting of Earth orbit ina particular direction or probably MMS spending most of its time in Northern hemisphere.

Furthermore, the distribution of various energy fluxes throughout the magnetotail varies significantly. As revealed in this study, in the Inner Plasma Sheet (IPS), the flux contributions follow the order: $EF > HF > SF > KE$, while in the Outer Plasma Sheet (OPS), they adhere to the order $SF > EF > HF > KE$. This observation suggests that each flux exhibits its own region of dominance within the magnetotail.

While this study does not delve into the specific physical mechanisms underlying the variation of energy fluxes across different cross-sections of Earth's magnetotail, it nonetheless provides an overall picture of the energy transport in this region. Exploring the underlying reasons for these variations will be the focus of our future investigations.

7 Acknowledgements

This research was supported by NASA Grant "NASA 80NSSC21K0580". We are thankful to the MMS team.

References

[1] V. Angelopoulos et al., "Statistical characteristics of bursty bulk flow events, " *JGR: Space Physics*, **99**, Nov, 1994, pp. 21257–21280, doi: 10.1029/94JA01263.

[2] C. C. Chaston et al., "Energy transport by kinetic-scale electromagnetic waves in fast plasma sheet flows, " *JGR: Space Physics*, **117**, Sep, 2012, pp. n/a–n/a, doi: 10.1029/2012JA017863.

[3] W. Baumjohann et al., "Average plasma properties in the central plasma sheet, " *JGR: Space Physics*, **94**, Jun, 1989, pp. 6597–6606, doi: 10.1029/JA094IA06P06597.

[4] C. T. Russell et al., "The Magnetospheric Multiscale Magnetometers, " *Space Science Reviews*, **199**, Aug, 2014, pp. 189–256, doi: 10.1007/s11214-014-0057-3.

[5] R. E. Ergun et al., "The Axial Double Probe and Fields Signal Processing for the MMS Mission, " *Space Science Reviews*, **199**, Dec, 2014, pp. 167–188, doi: 10.1007/s11214-014-0115-x.

[6] C. Pollock et al., "Fast Plasma Investigation for Magnetospheric Multiscale, " *Space Science Reviews*, **199**, Mar, 2016, pp. 331–406, doi: 10.1007/s11214-016-0245-4.

[7] H. Hasegawa, "Structure and Dynamics of the Magnetopause and Its Boundary Layers, " *Monographs on Environment, Earth and Planets*, **1**, Aug, 2012, pp. 71–119, doi: 10.5047/meep.2012.00102.0071.